JOURNAL OF Applied Polymer SCIENCE

Influence of Additive on Structure of PVDF Nanofibers Electrospun via New Spinneret Design

Yi Li, Masaya Kotaki
Department of Advanced Fibro-Science, Graduate School of Science and Technology, Kyoto Institute of Technology, Gosyokaido-cho, Matsugasaki, Sakyo-ku, Kyoto 606-8585, Japan
Correspondence to: M. Kotaki (E-mail: m-kotaki@kit.ac.jp)

ABSTRACT: Surface morphology and internal structure of polyvinylidene fluoride (PVDF) nanofibers were investigated in this study. PVDF nanofibers were electrospun by two types of spinnerets, nozzle and channel spinneret, with different contents of tetrabutylammonium chloride (TBAC) and at various take-up velocities. The new spinneret design, channel spinneret, resulted in thicker fibers while high β-phase content and small d-spacing were obtained, especially in the case of low TBAC content. And high TBAC content led to finer PVDF nanofibers with high β-phase content and small d-spacing compared to low TBAC content regardless of spinneret types, while an increase in take-up velocity did not have significant effect on both morphology and internal structure of PVDF nanofibers regardless of TBAC content. It suggests that electrostatic drawing acted dominantly rather than mechanically drawing in the system cooperating TBAC. However, the decreasing difference between two types of spinnerets was observed in terms of β-phase content with an increase in TBAC content. © 2013 Wiley Periodicals, Inc. J. Appl. Polym. Sci. 130: 1752–1758, 2013

KEYWORDS: fibers; morphology; crystallization

Received 10 November 2012; accepted 17 March 2013; Published online 6 May 2013
DOI: 10.1002/app.39336

INTRODUCTION

Poly(vinylidene fluoride) (PVDF) is widely used for industrial applications because of its excellent chemical stability, mechanical strength, and ferroelectricity. PVDF has at least four main crystalline structures: α-, β-, γ-and δ-phases, which are distinguished by the conformation of the C—C bond along the chain backbone.[1] Among four crystalline forms, the α-form (TGTG), the most common and stable form, is easily obtained by crystallization from quiescent PVDF, whereas the β-form, all-trans (TTTT), demonstrates the strongest pyro- and ferro-electric activity and are attracting when being applied as sensors or actuators.

The β-phase could be converted from α-phase or be induced directly via some special conditions. Many researchers have found that β-phase was transformed from α-phase with stretching films containing α-phase under special conditions,[2,3] the addition of both hydrofluoro-carbon solvent and ionic (anionic or cationic) fluorinated surfactant,[1,4] the addition of swift heavy ions,[5] sonication process in the mixture solution.[6] Ma et al. confirmed that molecular orientation is occurring during the electrospinning process itself.[7] Yee et al. found that compared with an increase in rotation speed and decrease in size of spinnerets, the effect of tetrabutylammonium chloride (TBAC) addition is more effectively compared with later two parameters. TBAC, a hygroscopic salt, could retain water in the fibers, which leads to hydrogen bonding between water molecules and the fluorine atoms of PVDF and hence more *trans* conformers.[8] Andrew et al. thought that low viscosity solution or under a high applied voltage for high viscosity solution[9] and the addition of nanoparticle phase could enhance the formation of PVDF phases.[6,10] Moreover, Rinaldo found that oriented β-phase are usually formed from uni- or biaxial mechanical drawing or originally α-phase films,[11] while nonoriented β-phase can be obtained from solution crystallization by slow evaporation of the solvent.[12,13]

Electrospinning, as a simple and versatile technique for producing nanofibers, has a high potential for structure control and a high capability for mass-production with different setup units. As known, nanosize scale properties may be different with conventional-scale properties. And one interesting aspect of electrospinning is that it allows the modification of fiber structure to be achieved by the manipulation of processing conditions and setup.

Among all the processing conditions, because of the great reliance on spinnerets in spinning methods,[14] spinneret is very vital when considering the effect of polymer chain behavior on final fiber structure. Rather than traditional nozzle spinneret, recently, needleless electrospinning appeared to be an attractive electrospinning technology with the original aim of improving productivity. Until now, various kinds of spinnerets, wire coil,[15]

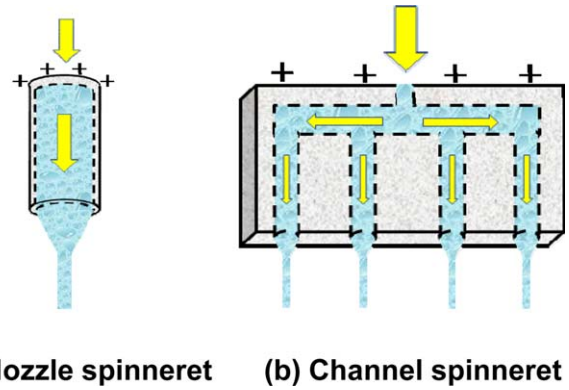

Figure 1. Schematic diagram of two spinneret design: (a) Nozzle spinneret, (b) Channel spinneret. [Color figure can be viewed in the online issue, which is available at wileyonlinelibrary.com.]

disk,[16] cylinder,[17] rotary cone,[18] and so on, were reported. It is found that the electric field distribution, as well as the electric field strength could affect the jet path efficiently among different spinnerets.[19] Lin et al. reported the spinneret geometry significantly affected the electrospinning process and fiber property.[20] Xie et al. found that the electric field strength in the spinneret tip and in the space between spinneret tip and collector have different effect on fiber diameter.[21] However, the control of fiber morphology and structure through different kinds of spinnerets has not been demonstrated in needleless electrospinning.

The aim of this study is to investigate the influence of electrospinning conditions, especially spinneret type, on morphology and structure formation of PVDF nanofibers. PVDF nanofibers in this study were electrospun from solutions of different TBAC contents and collected at various take-up velocities. In addition, new type of spinneret, channel spinneret, was adopted and compared with conventional nozzle spinneret.

EXPERIMENTAL

Materials

PVDF (Solef 21216) was used as polymer in this study. The electrospinning solutions were prepared by dissolving PVDF in *N,N*-dimethylformamide (DMF) with concentration of 8 and 12 wt%. In addition, TBAC was added into PVDF solution as additive. Its contents ranged from 0 phr (parts per hundreds of resin), 0.5, 1, to 2 phr in the case of 8 wt% solution system and 0 and 1 phr for 12 wt% system.

Electrospinning

The solutions were electrospun using NANON (MECC) at 23 kV by using two kinds of spinnerets, nozzle and channel spinneret (provided by MECC), as shown in Figure 1, with internal diameter of each hole of 0.3 mm. The feed rate was fixed at 1.0 mL $(h{\cdot}hole^{-1})^{-1}$. A drum collector was used to obtain aligned nanofibers in this study. Take-up velocities corresponding to the rotation speed of the disc collector varied from 630, 1260, to 1890 $m{\cdot}min^{-1}$ while a plate collector was chosen to collect random fibers, or fiber spun at 0 $m{\cdot}min^{-1}$. The gap between the tip of the spinneret and the surface of the collector was 15 cm. The electrospun nanofibers were dried in a desiccator for at least 24 h prior to use.

Morphology and Internal Structure Analysis

Fiber morphology was observed by using field emission scanning electron microscope (FE-SEM, Hitachi S4200). The nanofibers were prepared by first placing them on the vacuum and then coating the surface with gold.

Phase transformation was characterized by FTIR instrument (Perkin Elmer Spectrum GX). The FTIR spectra were scanned by transmission in the range of 450–1000 cm^{-1} with a resolution of 2.0 cm^{-1}. The laser beam was focused to a spot of area ~1 mm^2 on the fiber mat gathered on the collector. All spectra were acquired by 16 scans. For a system containing α- and β-

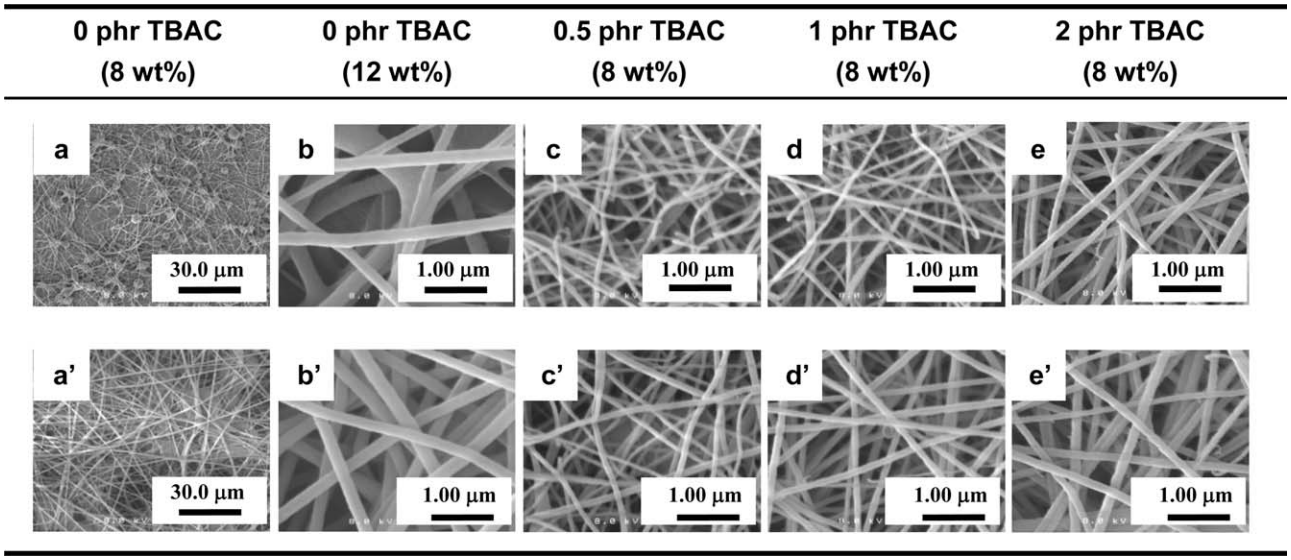

Figure 2. SEM images of PVDF random nanofibers prepared from solutions of different TBAC contents and by different spinnerets: a, b, c, d, and e: nozzle; a′, b′, c′, d′, and e′: Channel spinnerets. All fibers were collected at take-up velocity of 0 $m{\cdot}min^{-1}$.

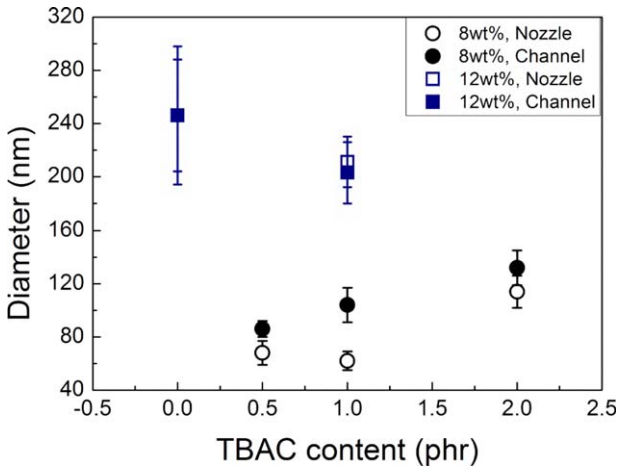

Figure 3. Relationship between average diameter of PVDF random fibers spun by different spinnerets and TBAC content of solution. [Color figure can be viewed in the online issue, which is available at wileyonlinelibrary.com.]

phases, the relative fraction of β-phase, $F(\beta)$, can be calculated by using eq. (1):

$$F(\beta) = \frac{X_\beta}{X_\beta + X_\alpha} = \frac{A_\beta}{1.3A_\alpha + A_\beta} \quad (1)$$

where A_α and A_β are corresponded to absorption bands at 765 and 840 cm^{-1} for α- and β-phase, respectively. None of the spectra presented have been smoothed.

Crystalline morphology within the fibers was characterized via wide angle X-ray diffraction (WAXD) using Cu Kα radiation (0.15 nm) generated at 40 kV and 40 mA. The 2θ scanning angle was between 5 and 30° by using SmartLab. The samples used for WAXD test were the same as that for FTIR test. To understand the variation of crystalline structure during electrospinning, lattice spacing (d) were evaluated by the Bragg equation as shown below:

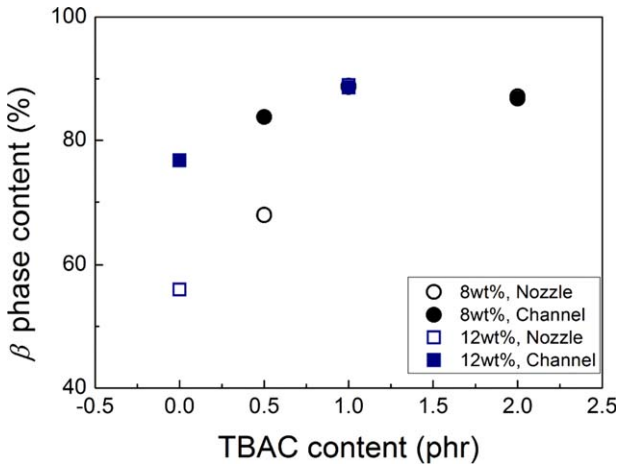

Figure 4. Relationship between β-phase content, $F(\beta)$, of PVDF random fibers spun by different spinnerets and from solution of various TBAC contents and polymer concentrations. [Color figure can be viewed in the online issue, which is available at wileyonlinelibrary.com.]

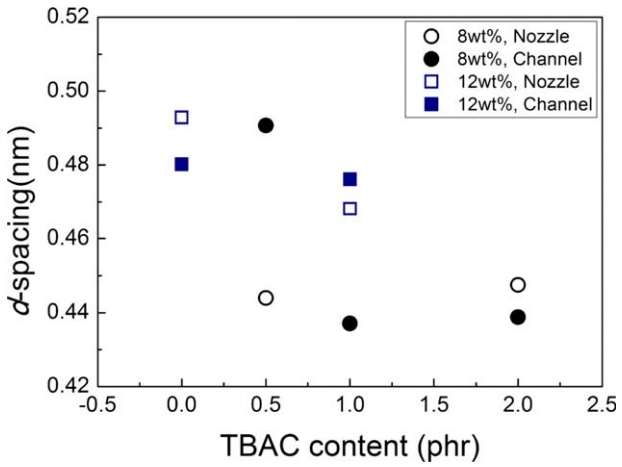

Figure 5. Relationship between d-spacing of PVDF random fibers spun by different spinnerets and from solution of various TBAC contents and polymer concentrations. [Color figure can be viewed in the online issue, which is available at wileyonlinelibrary.com.]

$$n\lambda = 2d\,Sin\,\theta \quad (2)$$

where n is an integer, λ is the wavelength of incident wave, d is the spacing between the planes in the atomic lattice, and θ is the angle between the incident ray and the scattering planes.

RESULTS AND DISCUSSION

TBAC Addition Effect

In this work, PVDF nanofibers were prepared from solutions of different TBAC contents and spun by nozzle and channel spinnerets, respectively. The PVDF nanofibers were collected by plate collector and take-up velocity was set as 0 $m{\cdot}min^{-1}$. The detailed electrospinning conditions are listed in Table 1. As shown in Figure 2, the concentration of solution without TBAC addition, or 0 phr TBAC addition, was increased from 8 to 12 wt% to obtain bead-free fibers. Besides, relationship between average diameter of PVDF nanofibers and TBAC was shown as Figure 3. It can be clearly observed that nozzle spinneret led to finer fibers and this difference was not obvious in the case of electrospinning solutions with high polymer concentration. Moreover, with TBAC content increasing, finer fibers were obtained from high viscosity solution while average diameter of fibers from low viscosity solution changed slightly. Specifically, In the case of high polymer concentration (12 wt%) solution, the deviation of nanofibers diameter from 0 phr TBAC system varies significantly compared with that from 1 phr system. And the average diameters of PVDF nanofibers were different between these two solution systems. The results are in accordance with previous results that high TBAC content led to the decrease of fiber diameter because of the conductivity of solution was increased.[8] And in the study, it is found that in high viscous solution, the effect of conductivity is more obvious when compared with that in low viscous solution.

The effect of TBAC content on crystalline phases of PVDF nanofiber can be further understood by FTIR and WAXD analysis (Table 1). β-phase content and d-spacing as a function of TBAC content were plotted and shown in Figures 4 and 5,

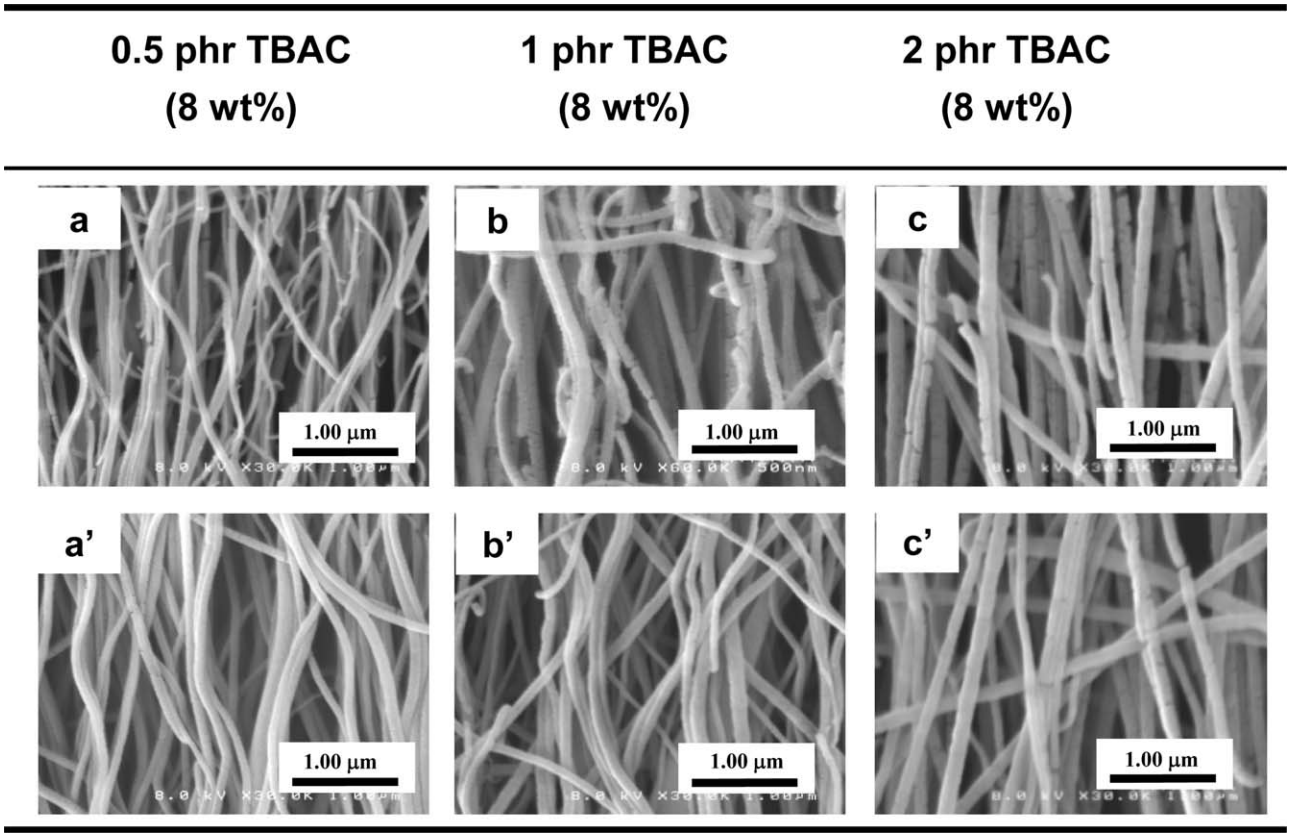

Figure 6. SEM image of PVDF nanofibers spun at take-up velocity of 1890 m min^{-1} by different spinneret and with different TBAC contents: (a), 0.5 phr, nozzle, (a′), 0.5 phr, channel, (b), 1 phr, nozzle, (b′), 1 phr, channel, (c), 2 phr, nozzle, (c′), 2 phr, channel. All the PVDF fibers were spun from solutions with polymer concentration of 8 wt %.

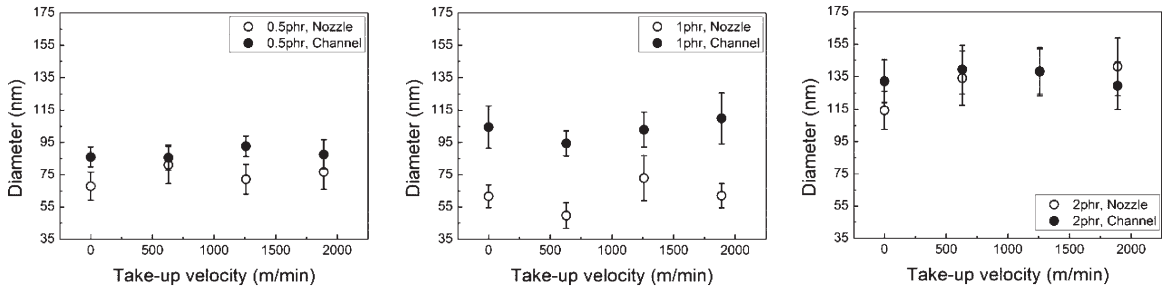

Figure 7. Relationship between diameter and take-up velocity of PVDF nanofibers spun by different spinnerets and with TBAC content.

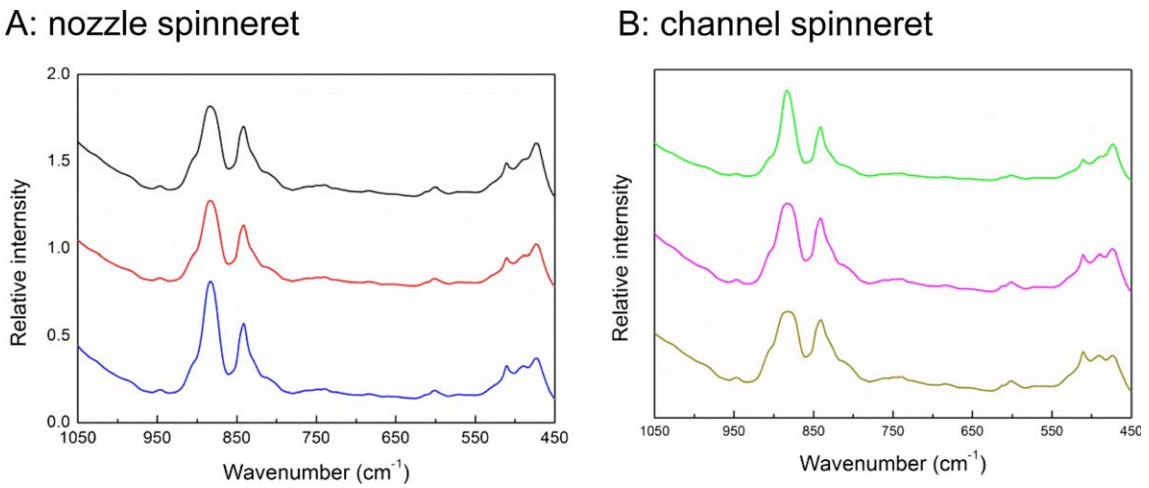

Figure 8. FTIR spectrum of PVDF nanofibers spun by (A) nozzle spinneret and (B) channel spinneret collected at take up velocities of (1) 630 m·min^{-1}, (2) 1260 m·min^{-1}, and (3) 1890 m·min^{-1}. The polymer concentration and TBAC content were fixed at 8 wt% and 2 phr, respectively. [Color figure can be viewed in the online issue, which is available at wileyonlinelibrary.com.]

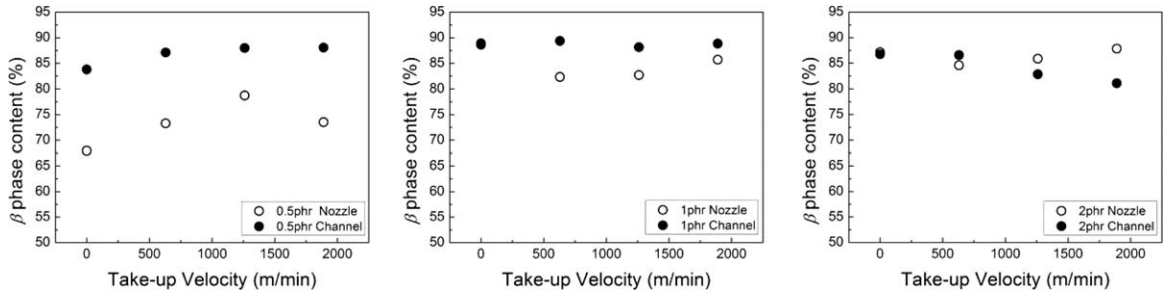

Figure 9. Effect of take-up velocity on β-phase content of PVDF fibers spun by different spinnerets and with different TBAC contents.

respectively. The results indicated that high TBAC content led to high β-phase content and smaller planar distance in β-phase regardless of viscosity of solution. However, the decrease in both $F(\beta)$ and d-spacing was more obvious in the case of solution of high viscosity compared with that of low viscosity. Thus, it can be concluded that the specific crystalline structure of β-phase, more *trans* conformers, presented more packed internal structure.

Take-up Velocity Effect

Figure 6 presents morphologies of PVDF nanofibers electrospun at 1890 m·min^{-1} with different TBAC contents by nozzle and channel spinnerets, respectively. The result indicated that nanofibers spun at high take-up velocity were broken fibers, while as-spun fibers presented the continuous morphology. The as-spun fibers were nanofibers obtained after placing on the vacuum for 12 h but without any other post processing, like gold coating. Therefore, the fibers were being broken in the gold coating process prior to the SEM observation. By comparing with continuous morphology of PVDF nanofibers collected at low take-up velocity (Figure 2), it is indicated that high take-up velocity resulted in more ordered internal structure and high residual strain as fibers were more easily to be broken. Moreover, according to Figure 7, the diameter of PVDF nanofibers varied slightly with an increase in take-up velocity regardless of spinneret type. And it showed that nozzle spinneret led to finer fibers regardless of take-up velocity.

Moreover, Figure 8 shows the FTIR spectrum of PVDF nanofibers with spun by nozzle spinneret and channel spinneret collected at different take up velocities, where the α-phase related bands can be observed at 765 cm^{-1} and β-phase at 840 cm^{-1}, respectively. To understand the effect of take-up velocity on internal structure of PVDF nanofibers, the relationships between β-phase content and take-up velocity is shown in Figure 9. It can be observed that with an increase in TBAC content, the difference in $F(\beta)$ between nozzle and channel spinnerets was decreased. However, the take-up velocity effect in fixed TBAC content is not very significant according to the FTIR analysis.

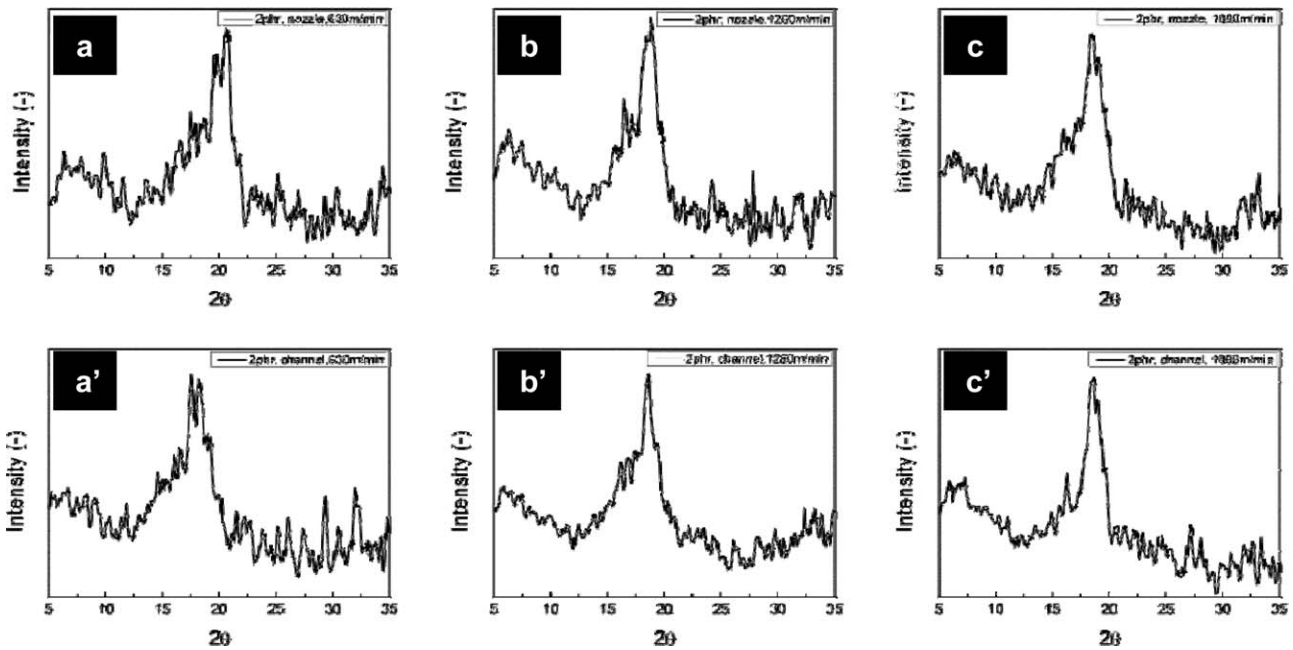

Figure 10. WAXD diffractograms of PVDF fibers electrospun with 2 phr TBAC by nozzle spinneret (a,b,c) and channel spinneret (a′, b′, c′) and collected using the rotating drum collector at: (a,a′) 630 m·min^{-1}, (b,b′) 1260 m·min^{-1}, (c, c′) 1890 m·min^{-1}. The PVDF concentration of all electrospinning solutions were 8 wt%.

Table I. Diameter, β-Phase Content, d-Spacing of PVDF Nanofibers Spun by Nozzle and Channel Spinneret and Different Solutions Systems.

Spinneret	Concentration (wt %)	TBAC content (phr)	Diameter (mm)	β-phase content (%)	d-spacing (nm)
Nozzle	8	0		Beaded	
		0.5	68 ± 9	67.972	0.4623
		1	62 ± 7	83.799	0.4405
		2	114 ± 12	87.168	0.4475
	12	0	246 ± 52	55.964	0.4860
		1	211 ± 19	89.367	0.4680
Channel	8	0		Beaded	
		0.5	86 ± 6	88.639	0.4440
		1	104 ± 13	88.911	0.4370
		2	132 ± 13	86.769	0.4388
	12	0	246 ± 42	76.728	0.4800
		1	203 ± 23	88.894	0.4760

All the nanofibers were collected at take up velocity of 0 m min $^{-1}$.

Table II. 2θ of PVDF Nanofibers Spun from Solutions with Different TBAC Content, by Different Spinnerets, and Collected at Different Take-Up Velocity

		0.5 phr TBAC	1 phr TBAC	2 phr TBAC
Spinneret	Take-up velocity (m min $^{-1}$)		2θ(°)	
Nozzle	0	20.00	20.32	19.84
	630	18.72	18.32	20.64
	1260	18.48	18.56	18.80
	1890	18.48	18.64	18.48
Channel	0	18.08	20.32	20.24
	630	17.92	18.72	18.16
	1260	18.64	18.48	18.64
	1890	18.96	18.56	18.64

All the PVDF nanofibers were fabricated from solution with concentration of 8 wt %.

Furthermore, the WAXD diffractograms and 2θ of the fibers electrospun from the PVDF solutions containing 2 phr TBAC collected at different take-up velocity are shown in Figure 10 and Table II, respectively. Based on WAXD data, it was found that some of crystallized PVDF in the study showed a well-defined single peak at around $2\theta = 20.3°$, referred to the sum of the diffractions in plane (110) and (200) characteristic of β-phase, and some were at $2\theta = 18.4°$, related to the diffractions in (020) plane indicating the dominance of α-phase.[11] Although it is difficult to distinguish these two phases as there is a common peak around 20°, Figure 11 presents the relationship between planar distance in α- or β-phase and take-up velocity of fiber spun by different spinneret and collected at take-up velocities. It was illustrated that an increase in take-up velocity led to *d*-spacing decreasing regardless of crystalline phase in PVDF nanofibers.

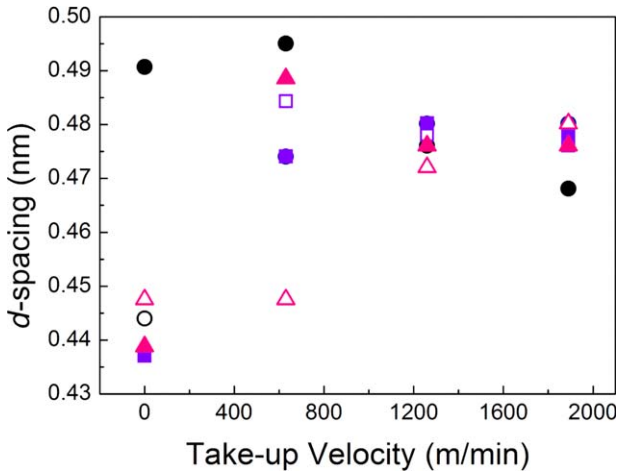

Figure 11. Relationship between *d*-spacing with take-up velocity in terms of α- and β-phase; ○: 0.5 phr, nozzle spinneret; ●: 0.5 phr, channel spinneret; □: 1 phr, nozzle spinneret; ■: 1 phr, channel spinneret; △: 2 phr, nozzle sipnneret; ▲: 2 phr, channel spinneret. [Color figure can be viewed in the online issue, which is available at wileyonlinelibrary.com.]

CONCLUSIONS

In this study, it was demonstrated that spinneret type, TBAC addition and take-up velocity affected the structure of PVDF

nanofibers. As for the effect of TBAC content, the results showed that with increasing in TBAC content in electrospinning solution, finer PVDF nanofibers were obtained as well as packed structure of small *d*-spacing with high *β*-phase content. And this effect was more obvious in the case of solution of high viscosity, which might be related to viscoelastic and electrostatic force when polymer jet was travelling from top of spinneret to the collector. Besides, the effect of take-up velocity on PVDF structure, morphology, *β*-phase as well as *d*-spacing was not very significant. Therefore, it suggests that electrostatic drawing acted dominantly rather than mechanically drawing in the electrospinning system with TBAC addition. But the difference between nozzle and channel spinneret was small in terms of *β*-phase content with TBAC content increasing regardless of take-up velocity.

ACKNOWLEDGMENTS

The authors thank MECC Co., Ltd. for both the financial and technical support.

REFERENCES

1. Nasir, M.; Matsumoto, H.; Danno, T.; Minagawa, M.; Irisawa, T.; Shioya, M.; Tanioka, A. *J. Polym. Sci. B Polym. Phys.* **2006**, *44*, 779.
2. Khakhar, D. V.; Misra, A. *J. Appl. Polym. Sci.* **2010**, *117*, 3491.
3. Sencadas, V.; Gregorio, R., Jr.;Lanceros-Mendez, S. *J. Macromol. Sci.* **2009**, *48*, 514.
4. Nasir, M.; Matsumoto, H.; Minagawa, M.; Tanioka, A.; Danno, T.; Horibe, H. *Polym. J.* **2007**, *39*, 670.
5. Nitanan, T.; Opanasopit, P.; Akkaramongkolporn, P.; Rojanarata, T.; Ngawhirunpat, T.; Supaphol, P. *Korean J. Chem. Eng.* **2012**, *29*, 173.
6. Yu, S.; Zheng, W.; Yu, W.; Zhang, Y.; Jiang, Q.; Zhao, Z. *Macromolecules* **2009**, *42*, 8870.
7. Ma, X.; Liu, J.; Ni, C.; Martin, D. C.; Chase, D. B.; Rabolt, J. F. *ACS Macro Lett.* **2012**, *1*, 428.
8. Yee, W. A.; Kotaki, M.; Liu, Y.; Lu, X. *Polymer* **2007**, *48*, 512.
9. Andrew, J.; Clarke, D. *Langmuir* **2008**, *24*, 670.
10. Andrew, J.; Clarke, D. *Langmuir* **2008**, *24*, 8435.
11. Gregorio, R., Jr.;Ueno, E. M. *J. Mater. Sci.* **1999**, *34*, 4489.
12. Gregorio, R., Jr.;Cestari, M. *J. Polym. Sci. B Polym. Phys.* **2003**, *32*, 859.
13. Gregorio, R., Jr.; Borges, D. S. *Polymer* **2008**, *49*, 4009.
14. Shambaugh, R. L. *Indus. Eng. Chem. Res.* **1988**, *27*, 2363.
15. Wang, X.; Niu, H.; Wang, X.; Lin, T. *J. Nanomater.* **2012**, *3*, 2012.
16. Niu, H.; Lin, T.; Wang, X. *J. Appl. Polym. Sci.* **2009**, *114*, 3524.
17. Wu, D.; Huang, X.; Lai, X.; Sun, D.; Lin, L. *J. Nanosci. Nanotechnol.* **2010**, *10*, 4221.
18. Lu, B.; Wang, Y.; Liu, Y.; Duan, H.; Zhou, J.; Zhang, Z.; Wang, Y.; Li, X.; Wang, W.; Lan, W.; Xie, E. *Small* **2010**, *6*, 1612.
19. Ying, Y.; Zhidong, J.; Qiang, L.; Jianan, L.; Zhicheng, G. *Dielectrics Electrical Insulation* **2009**, *16*, 409.
20. Wang, X.; Niu, H.; Lin, T.; Wang, X. *Polymer Engineering & Science* **2009**, *49*, 1582.
21. Xie, S.; Zeng, Y. *Indus. Eng. Chem. Res.* **2012**, *51*, 5336.